

# Human–Robot Interaction Evaluation-Based AAN Control for Upper Limb Rehabilitation Robots Driven by Series Elastic Actuators

Shuaishuai Han<sup>✉</sup>, Haoping Wang<sup>✉</sup>, Senior Member, IEEE, and Haoyong Yu<sup>✉</sup>, Senior Member, IEEE

**Abstract**—Series elastic actuators (SEAs) have been the most popular compliant actuators as they possess a variety of advantages, such as high compliance, good backdrivability, and tolerance to shocks. They have been adopted by various rehabilitation robots to provide appropriate assistance with suitable compliance during human–robot interaction. For a multijoint SEA-driven rehabilitation robot, a big challenge is to develop an assist-as-needed (AAN) method without losing stability during uncertain physical human–robot interaction. For this purpose, this article proposes a human–robot interaction evaluation-based AAN method for upper limb rehabilitation robots driven by SEAs. First, in order to stabilize the SEA-level dynamics, singular perturbation theory is adopted to design a fast time-scale controller. Second, for the robot-level dynamics, an iterative learning algorithm is adopted for impedance adaption according to the task performance and human intention. The interaction force feedback is introduced for human–robot interaction evaluation, and the intensity of robotic assistance will be adjusted periodically according to the evaluation results. The stability of human–robot interaction is provided with the Lyapunov method. Finally, the proposed rehabilitation method is constructed and implemented on a two-degree-of-freedom SEA-driven robot. It handles the uncertain interaction in such a principle that correct movements will lead to less assistance for encouraging participation and incorrect movements will lead to more assistance for effective training. The proposed method adapts to the subject’s intention and encourages higher participation by decreasing impedance learning strength and increasing allowable motion error. It can fit the participants with different motor capabilities and provide adaptive assistance when a specific trainee tries to change his/her participation during rehabilitation. The performance of the AAN method was validated with experimental studies involving healthy subjects.

Manuscript received 28 September 2022; revised 17 January 2023; accepted 15 March 2023. This paper was recommended for publication by Associate Editor C. Yang and Editor E. Yoshida upon evaluation of the reviewers’ comments. This work was supported in part by the Agency for Science, Technology and Research (A\*STAR), Singapore, under the National Robotics Program, with A\*STAR Science and Engineering Research Council under Grant 1922500054, and in part by the National Natural Science Foundation of China under Grant 62173182 and Grant 61773212. (*Corresponding authors:* Haoping Wang; Haoyong Yu.)

Shuaishuai Han is with the School of Automation, Nanjing University of Science and Technology, Nanjing 210094, China, and also with the Department of Biomedical Engineering, National University of Singapore, Singapore 117583 (e-mail: ss.han@njust.edu.cn).

Haoping Wang is with the School of Automation, Nanjing University of Science and Technology, Nanjing 210094, China (e-mail: hp.wang@njust.edu.cn).

Haoyong Yu is with the Department of Biomedical Engineering, National University of Singapore, Singapore 117583 (e-mail: biehy@nus.edu.sg).

Color versions of one or more figures in this article are available at <https://doi.org/10.1109/TRO.2023.3286073>.

Digital Object Identifier 10.1109/TRO.2023.3286073

**Index Terms**—Assist-as-needed (AAN), human–robot interaction, impedance adaption, series elastic actuator (SEA)-driven robot.

## I. INTRODUCTION

**S**TROKE and traumatic brain injury leave millions of survivors with physical disabilities, which result in great demands for rehabilitation. Traditional therapies need great labor intensity, and they usually suffer from bad repetition and low efficiency. This gives rise to the research on robot-assistance rehabilitation, which can greatly release the medical pressure during task-oriented rehabilitation [1]. Lots of previous works, like MIT-MANUS upper limb rehabilitation robot [2] or LOKOMAT lower limb exoskeleton [3], have demonstrated great potential and efficiency of the robot-assistance rehabilitation.

A large number of upper limb rehabilitation robots are driven by rigid joints [4], [5], [6] and operate motion guidance during training tasks [5]. With rigid-joint rehabilitation robots, precise position control-based training can be well achieved, and interaction effects are usually viewed as disturbance [7] to be eliminated. However, rigid-joint robots can hardly handle or absorb possible high-frequency fluctuations from human movements. The high mechanical stiffness and low backdrivability may cause stumbles when the trainee tries to voluntarily move.

For overcoming some intrinsic limitations from rigid robots, compliant actuator-driven robots have become a popular choice during human–robot interactive applications [8]. Among these robots, series elastic actuator (SEA)-driven robots [9], [10], [11] have become increasingly attractive because of their superior advantages in physical human–robot interaction (pHRI), such as high force/torque fidelity, high compliance, good backdrivability, and tolerance to shocks. These qualities bring in higher flexibility of control design and human–robot safety. In [11], a lightweight SEA-driven elbow rehabilitation robotic exoskeleton was designed, and some primary tests were conducted including force controllability and transparency. In [12], a single-joint SEA-driven robot was applied for upper limb rehabilitation, and an impedance controller was proposed to achieve stable motion control.

However, existing studies on SEA-driven robots commonly focus on motion control (force control, position control, or impedance control) [11], [13], [14] or limited to single-joint condition [12], [15], [16]. The problem will become much more

complex when we try to extend the tasks to the robot-aided rehabilitation with two-joint or multijoint SEA-driven robots [17]. First, nonlinear coupling dynamics and mechanical compliance introduces unwanted intrinsic oscillatory dynamics, low bandwidth, and high-order dynamics with underactuation, which make it challenging to achieve stable and effective human–robot interaction control during rehabilitation [17]. Second, for maximizing the rehabilitation efficiency and taking advantages of the SEA-driven robot during rehabilitation, the assistance method obeying assist-as-needed (AAN) principles should be designed with the consideration of real-time physical interaction process. Such principles also become necessary requirements for advanced rehabilitation control for the patients with partially active motor ability [3], [18], [19].

For achieving efficient and active rehabilitation with SEA-driven robots, a stable controller under AAN principles needs to be developed. Most of the current AAN methods are inspired by the impedance concept, which has been a crucial method to perform robot-interactive tasks since proposed in [20]. Force field-based rehabilitation control, which was proposed in [21], is a typical AAN method for upper limb or lower limb rehabilitation [22], and it is also known as path control [23]. In this method, a virtual impedance wall is designed according to a target motion tunnel, in which human’s flexible active movements are allowed. The force field method has been shown to be more effective than strict predefined trajectory tracking method [24]. However, the system stability is not ensured, and manually regulated impedance parameters may only suit for a specific subject.

The multimode rehabilitation strategy [25], [26] guarantees the closed-loop stability by applying Lyapunov theory, and it addresses the safety problem during rehabilitation. The assistive ways or levels are designed according to different motion regions, which are predefined before operations. In [25], interaction force feedback was used to design a compensation term according to the force direction. However, the human motion performance or intention was not clearly evaluated, and real-time compensation with interaction force may not be the best way as it may lead to unwanted interaction results. In [26], interaction force was detected to determine the safety switching. Unfortunately, human intention or motion performance was only evaluated with motion errors in [26]. This leads to less flexibility, as when the motion regions or force field are constructed, the assistance that adapts only according to human’s motion and real-time interaction is not sufficiently evaluated.

As shown in [27], interaction force measure can be used for human intention evaluation and also for safety. It can release the requirement of modeling accuracy for human–robot interaction estimation. Primary work can be found in [27], in which the human–exoskeleton interaction forces were measured during each gait period and evaluated for adapting the reference trajectory of next gait period. In this way, human’s moving intention can be clearly detected, and active engagement will be promoted with proper gait leading. Therefore, we claim that it is more reasonable to evaluate the human intention during each operation and adjust the assistance level at next operation accordingly. In [18], [28], human–robot interaction forces were

estimated with precise robot dynamic modeling or identification by neural networks and used for assistance adaption during each operation. A force decay method similar to the work in [29] and an error region adaption idea were adopted to realize AAN target and promote the trainee’s active engagement. However, the large number of neural networks (125 radial basis functions in [28]) requires high-quality processor, and precise dynamic modeling is more difficult for a multijoint SEA-driven robot.

As demonstrated in [30], human joints and endpoints will iteratively adapt their impedance or stiffness when interacting with stable/unstable environment. Human beings use a learning method during repetitive tasks to acquire motion stability and achieve minimum motion error and minimum effort at the same time [30]. If a rehabilitation robot possesses similar learning properties of the human limbs, it will benefit the rehabilitation [31], [32].

In this article, the human-like iterative learning idea [31] is adopted to possess the robot learning ability during repetitive tasks. Instead of rigidly correct the trainee’s motion, the proposed method for the SEA-driven robot can iteratively correct the motion with high compliance, which will benefit the motor recovery in a human-like way. For stable performing of the entire system, singular perturbation theory [33], [34] is applied to stabilize the SEA-level dynamics. Then, for the robot-level dynamics, an impedance learning algorithm is designed to approach the minimal required efforts from the robot and handle the unpredictable human–robot interactions. In order to further enhance the flexibility of assistance process, additional adjustment factors are introduced to the iterative learning algorithm and a robust control term. The adjustment factors will periodically adapt to the human intention, which is evaluated with human–robot interaction forces.

The main contributions of this article lie in the proposed human–robot interaction evaluation-based AAN method for upper limb rehabilitation robots driven by SEAs. Such a method is constructed by introducing the impedance learning algorithm and real-time interaction force measuring. Through real-time impedance learning and periodical adjustment, the proposed method can adapt the assistance level according to the rehabilitation performance and human intention. Through suitable evaluation of the human–robot interaction process, the rehabilitation robot can fit the trainee with different participation levels. Besides, the human–robot system stability is theoretically guaranteed under Lyapunov theory. Finally, the proposed AAN method is successfully implemented and validated on a multijoint SEA-driven robot, whose low mechanical stiffness possesses its intrinsic superiors in human–robot interaction. The trainee can freely change the moving effort without losing stability, and the adaption method helps to recover the motion performance and encourage active participation.

The rest of this article is organized as follows. Section II describes a multijoint SEA-driven robot and the system dynamics. The design and analysis of the proposed AAN method are described in Section III. The experimental evaluation of the AAN strategy is presented in Section IV. Finally, Section V concludes this article.

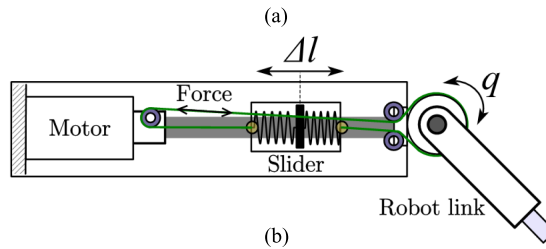
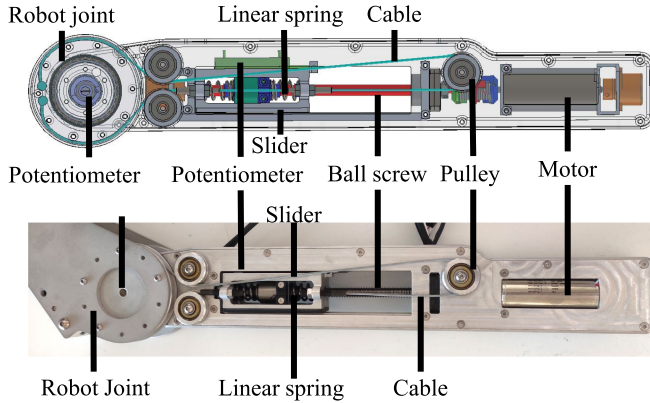


Fig. 1. (a) Mechanical structure of the SEA. (b) Working principle of the SEA. By introducing the ball screw, the rotary motion of the motor is converted to the linear motion of the ball screw nut. The ball screw nut will compress the springs and drive the slider, which will further drive the joint rotation through cables. With such transmission, the actuation mechanism will feature the compliance from springs. Besides, ball screw is playing the role of a reducer. The developed SEA is a compact and modular device, which can be utilized in different robotics.

## II. SEA-DRIVEN ROBOT

### A. Hardware Configurations

A compact and modular SEA is studied in this article. Fig. 1 shows the mechanical structure and working principle of the SEA. The SEA mainly consists of a driven motor (EC-4pole 30, brushless, 200 W, Maxon, Switzerland) with 92.9-mN·m nominal torque (maximal continuous torque), two linear springs, a ball screw, a linear potentiometer to measure the deformation of the linear spring, and a torsional potentiometer to measure the position of the robot joint. The motor transmits force to the cables via the springs. The cables exert torque on the robot joint by means of a pulley and a fixed-axis rotary coupling. The springs ensure that the coupling between the user and the motor is compliant, thereby protecting the users body from impact loads and other undesirable interactions. Similar mechanism can also be found in our previous research [15], [35]. Some basic specifications are summarized in Table I. According to the working principle of the SEA shown in Fig. 1, the nominal force applied on the cable can be computed as  $92.9 \text{ mN} \cdot \text{m} \times (2\pi/p) = 291.7 \text{ N}$ , where  $p$  is the pitch of the ball screw. Thus, the nominal torque applied on the robot joint is  $291.7 \text{ N} \times r = 10.21 \text{ N} \cdot \text{m}$ , where  $r$  is the radius of the robot joint, which means the distance between joint center and the cable. By denoting spring stiffness as  $k_l$  and compressed deformation of spring as  $\Delta l$ , the force on the cable can be computed and measured as

$$F = k_l \Delta l. \quad (1)$$

TABLE I  
PHYSICAL SPECIFICATIONS

Symbol	Quantity	Value
$p$	Pitch of the ball screw	$2 \times 10^{-3} \text{ m}$
$k_l$	Stiffness of the spring	$24 \times 10^3 \text{ N/m}$
$r$	Radius of the robot joint	$3.5 \times 10^{-2} \text{ m}$
$m_1$	Mass of link 1	1.1 kg
$m_2$	Mass of link 2	0.4 kg
$l_1$	Length of link 1	0.37 m
$l_2$	Length of link 2	0.285 m
$k$	Stiffness of SEA	29.4 N·m/rad
$J_{SEA}$	Inertia of SEA	$0.1562 \text{ kg} \cdot \text{m}^2$

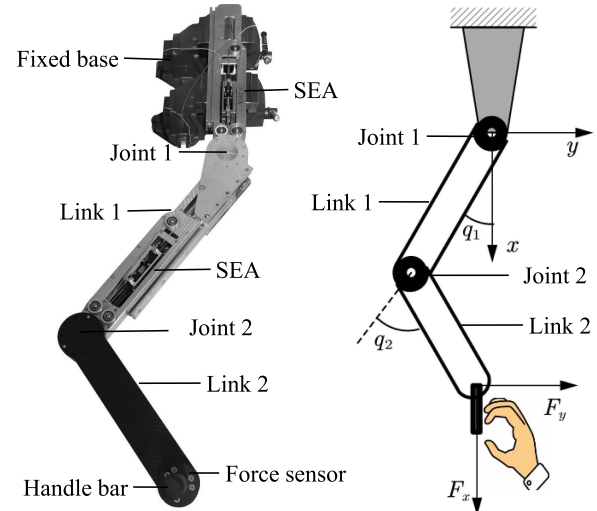


Fig. 2. Two-DOF SEA-driven robot: hardware components (left) and kinematic configurations (right). Cartesian coordinate, joint coordinate, and the coordinate of the end-effector interaction force are defined.

Then, the applied torque on the robot joint is  $k_l \Delta l \times r$ . According to the working principle of the SEA, the equivalent joint stiffness is  $k_l \times r^2 = 29.4 \text{ N} \cdot \text{m}/\text{rad}$ , which is denoted as  $k$  in Table I.

By utilizing the SEA, a two-degree-of-freedom (DOF) SEA-driven robot is set up and shown in Fig. 2, which will be applied to the upper limb rehabilitation assistance in this study. A force sensor (Mini58, ATI Industrial Automation, Apex, NC, USA) is equipped under the handlebar for the interaction force measuring. The central processor is equipped with the dSPACE 1007 control board with the DS2102 digital-to-analog converter board to generate control commands and the DS2002 analog-to-digital converter board to collect potentiometer signals. Each motor is driven by an Elmo driver (Gold DC Whistle, Petach Tikva, Israel). The physical parameters of this SEA-driven robot are also summarized in Table I.

A two-DOF SEA-driven robot will possess strong nonlinearity and coupling, which are general and crucial features of multijoint robots. For rehabilitation training, a two-DOF robot is a common choice for upper limb training, and it can help complete most of the planar tasks. Typical tasks like reaching between points can be well defined with such a robot. Therefore, it will be a suitable setup for evaluating the proposed AAN control approach. Besides, the current setup is only for the validation of the proposed control approach. It is not an optimized

rehabilitation robot for clinical applications. In the next phase of our work, a new prototype for clinical trials will be developed.

### B. Dynamic Modeling

According to [26], [36], the dynamics of an SEA-driven robot interacting with human can be formulated as

$$\begin{aligned} M(q)\ddot{q} + C(q, \dot{q})\dot{q} + G(q) &= K(\theta - q) + \tau_h \\ \ddot{\theta} + K(\theta - q) &= u \end{aligned} \quad (2)$$

where  $q = [q_1 \dots q_n] \in R^n$  is the vector of robot joint angles and  $\theta = [\theta_1 \dots \theta_n] \in R^n$  is the vector of the actuator angles.  $n$  denotes the number of actuated joints.  $M(q)$ ,  $C(q, \dot{q})$ , and  $G(q)$  denote the inertial matrix, the centroid and Coriolis force matrix, and the gravity force vector, respectively.  $M(q) - 2C(q, \dot{q})$  is a skew-symmetric matrix.  $\tau_h$  denotes a torque vector exerted by human hand.  $K = \text{diag}\{k \dots k\}$  is a matrix composed of the SEA stiffness coefficient  $k$ .  $J = \text{diag}\{J_{\text{SEA}} \dots J_{\text{SEA}}\}$  is composed of the equivalent inertia  $J_{\text{SEA}}$  of the SEA.  $u$  denotes the control torque from the driven motor.

Equation (2) consists of the robot-level dynamics and the SEA-level dynamics. The driven torque vector  $K(\theta - q)$  in robot-level dynamics is generated from the SEA-level dynamics. The entire SEA-driven robot dynamics is fourth-order and highly nonlinear. In fact, (2) is an equivalent dynamic model because the linear potentiometers only measure spring deformation  $\Delta l$ , as shown in Fig. 1(b), instead of the actuator angles. During practical implementations, the spring deformation is converted to be the actuator angle as  $\theta = q + \Delta l/r$ .

From [31], [37], the moving characteristics of a human's upper limb with a target trajectory during interactive conditions, no matter impaired or not, can be described in an impedance form as

$$\tau_h = \tau_0(t) + K_h(t)e + D_h(t)\dot{e} \quad (3)$$

where  $e = q_d - q$  and  $\dot{e} = \dot{q}_d - \dot{q}$  denote motion error vector and its first derivative between desired motion  $q_d$ ,  $\dot{q}_d$  and actual motion  $q$ ,  $\dot{q}$ . This is a basic and common model for describing the dynamic property of human motion, not a specific human motion model. Different from most of the assumptions in the existing publications where the optimal impedance parameters are assumed to be constant [12], [38], here, the impedance parameters  $K_h(t)$  and  $D_h(t)$  are more practically assumed to be time varying with a time-varying feedforward item  $\tau_0(t)$ .

For a multijoint SEA-driven rehabilitation robot with low stiffness, human–robot interaction will be compliant and smooth. However, the mechanical compliance introduces unwanted intrinsic oscillatory dynamics, low bandwidth, and high-order dynamics with underactuation, which make it challenging to achieve stable and effective rehabilitation control [17]. Besides, the unpredictable and uncertain human–robot interaction makes the entire system tend to be unstable.

### III. HUMAN–ROBOT INTERACTION EVALUATION-BASED AAN METHOD

In this section, we address the problem of designing an AAN rehabilitation strategy with SEA-driven robots that achieves following characteristics. For a given repetitive rehabilitation task (e.g., reaching task in this article), based on the human intention evaluation with interaction force measuring during current operation, the robot will adjust the assistive level at the initial of next operation by updating the control parameters. If the trainee can hardly finish the task or does not understand the task very well at the beginning, the robot will periodically enhance the assistance to encourage the trainee to learn the rehabilitation task. If the trainee can positively participate the rehabilitation and can almost independently finish the task, the robot will not increase or decrease the assistance. If the trainee tries to further increase his/her participation by adding higher interaction to the target direction, the robot will decrease the assistance and allow larger motion error, so that the trainee can get more motion freedom. The trainee can freely change the participation level without losing system stability.

Based on the ideas above, a human–robot interaction evaluation-based AAN control scheme is proposed and illustrated in Fig. 3. First, for stabilizing the SEA-level dynamics, a singular perturbation approach is adopted to design a *fast-time* controller  $u_{\text{fast}}$ , which will be introduced in detail in Section II-I-A. Then, for achieving the AAN target, a robot-level controller is developed, which is composed of a baseline control term  $u_{\text{ref}}$ , an impedance learning control term  $u_{\text{learn}}$ , and a robust term  $u_{\text{stable}}$ . The robot-level control structure will be introduced in Section III-B. In order to adapt the assistance from the robot, pHRI is periodically evaluated by measuring interactive force  $F_{\text{int}}$ . The impedance learning strength of  $u_{\text{learn}}$  and stable region of  $u_{\text{stable}}$  are periodically updated according to evaluation results. The evaluation and updating principles will be given in Sections III-C and III-D. Finally, Section III-E gives the stability analysis of the human–robot interaction system under the proposed AAN control.

#### A. SEA-Level Control

From the physical structure and SEA-driven robotic dynamics in (2), we can know that the SEA-level dynamics is directly driven by motor. The robot-level dynamics is driven by the output torque of the SEA. The entire robot dynamics is underactuated and physically compliant. For the motion control of such a plant, related work can be found originally in the publications on the control of flexible-joint robot, and some of the methods have been implemented on the SEA-driven robots [33]. Some well-known control methods include proportional–derivative (PD) control [39], passivity-based control [40], [41], model-inverse control (feedback linearization control) [42], etc. PD control and passivity-based control mainly focus on the regulation tasks when rigorous stability is required. Model-inverse control requires precise modeling information and will need extra approaches to treat possible disturbances like interactions with environment or human. Besides, the high-order and underactuated

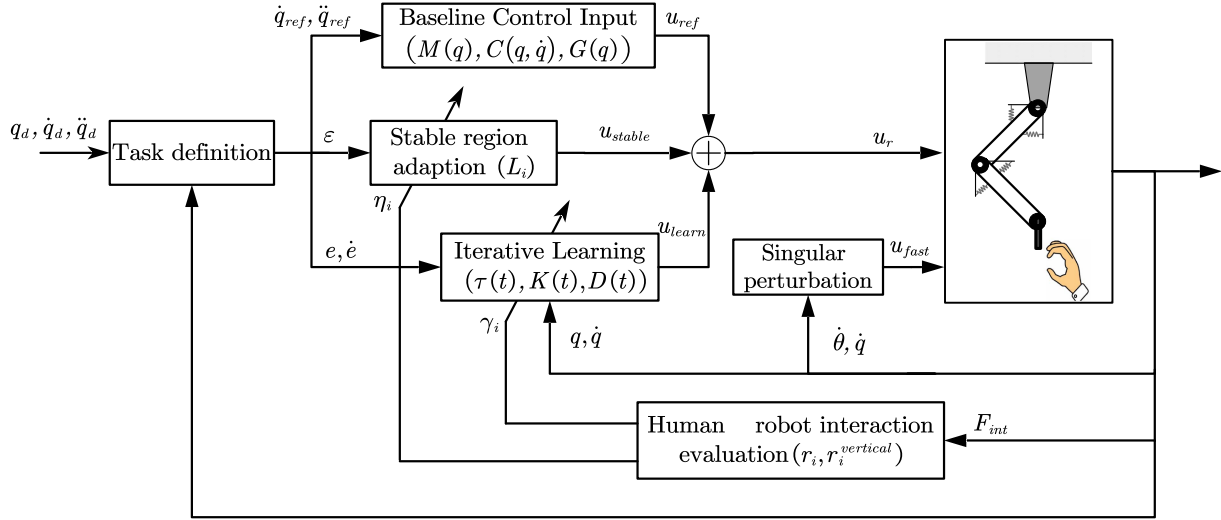


Fig. 3. AAN rehabilitation method with human–interaction evaluation: singular perturbation theory is used to design an SEA-level controller  $u_{\text{fast}}$ ; the baseline control term  $u_{\text{ref}}$  is used to guarantee effective movement of the robot; the interaction force is measured to evaluate human intention; the robust term  $u_{\text{stable}}$  is updated periodically and iterative learning rate for  $u_{\text{learn}}$  is adapted with human interaction evaluation.

dynamics lead to difficulties in extending existing robotic control methods to the SEA-driven robots. Comparatively, singular perturbation theory provides a convenient way for control design and stability analysis as it separates the higher order system to two lower order dynamic systems [34]. This makes it easier to extend existing robot-level control concepts to the SEA-driven robots.

For explaining the singular perturbation theory, we introduce the standard singular perturbation model first, which is state model where derivatives of some of the states are multiplied by a small positive parameter  $\delta$ , that is,

$$\dot{x} = f(t, x, z, \varepsilon) \quad (4)$$

$$\delta \dot{z} = g(t, x, z, \delta). \quad (5)$$

In (4) and (5),  $f$  and  $g$  are general functions and continuously differentiable in their arguments for  $(t, x, z, \delta) \in [0, t_1] \times D_x \times D_z \times [0, \delta_0]$ , where  $D_x \subset R^n$  and  $D_z \subset R^m$  are open connected sets. When we set  $\delta = 0$  in (4) and (5), the dimension of the state equation reduces from  $n + m$  to  $n$  because the differential equation (5) degenerates into the equation

$$0 = g(t, x, z, 0). \quad (6)$$

The model (4)–(5) is called standard singular perturbation model if (6) has and only has isolated real roots

$$z = h(t, x). \quad (7)$$

This assumption ensures that a well-defined  $n$ -dimensional reduced model will correspond to each root of (6). By substituting (7) into (4), at  $\delta = 0$ , the following reduced-order dynamics can be obtained

$$\dot{x} = f(t, x, h(t, x), 0). \quad (8)$$

This model is also called *quasi-steady-state model*, because  $z$ , whose velocity  $\dot{z} = g/\delta$ , can be large when  $\delta$  is small and  $g \neq 0$

may rapidly converge to a root of (6), which is the equilibrium of (8). Therefore, the dynamics (4) shows “slow” property with variable  $x$ , and the dynamics (5) shows “fast” property with variable  $z$ . The two-time-scale property of dynamics (4) and (5), which are also called slow model and fast model, gives the chance to analyze the high-order dynamics by analyzing the two models separately. The consequent problem is modeling a physical system in the singular perturbed form. However, there is no general principle for picking the small parameter  $\delta$ , and it is usually chosen according to our understanding to the physical processes and components [34], [43].

According to the working principles of the SEA, the SEA-level motion dynamics will be much faster than robot-level motion dynamics because of the inertial difference and compliant transmission.

For the SEA-level dynamics, we introduce a damping term  $u_{\text{fast}}$  to damp out the oscillatory dynamics [44], and the control law can be preliminarily written as

$$u = u_r + u_{\text{fast}}, u_{\text{fast}} = -K_{\text{fast}} (\dot{\theta} - \dot{q}) \quad (9)$$

where  $K_{\text{fast}} = \text{diag}\{k_{\text{fast}} \dots k_{\text{fast}}\}$  is a gain matrix and  $u_r$  is the robot-level controller which will be introduced later. By substituting (9) into the SEA-level dynamics in (2), one can obtain following results:

$$J\ddot{\theta} + K_{\text{fast}} (\dot{\theta} - \dot{q}) + K(\theta - q) = u_r. \quad (10)$$

By defining the variable  $z = K(\theta - q)$  denoting the joint torque provided by the SEA, the following equality holds:

$$\theta = K^{-1}z + q. \quad (11)$$

As  $J$ ,  $K_{\text{fast}}$ , and  $K$  are diagonal positive-definite matrices, by substituting (11) into (10), one has

$$\ddot{z} + K_{\text{fast}} J^{-1} \dot{z} + K J^{-1} z = K J^{-1} (u_r - J \ddot{q}). \quad (12)$$

As the damping coefficient  $K_{\text{fast}}$  can be artificially chosen, the value of  $KJ^{-1}$  determines if the SEA-level dynamics has faster response than the robot-level dynamic. Here, the key assumption for the application of singular perturbation theory to the SEA-driven robot is that  $KJ^{-1}$  is a matrix with high value elements. From the physical parameters in Table I, this assumption holds because of  $\frac{k}{J_{\text{SEA}}} = \mathcal{O}(100)$ , where the operator  $\mathcal{O}(\cdot)$  means the value of the same magnitude as its argument. Then, we may write

$$KJ^{-1} = \frac{1}{\delta^2} K_p, \quad K_{\text{fast}} J^{-1} = \frac{1}{\delta} K_d \quad (13)$$

where

$$K_p = \text{diag}\{k_p \dots k_p\}, \quad K_d = \text{diag}\{k_d \dots k_d\}$$

are positive-definite parametric matrixes with  $k_p, k_d = \mathcal{O}(1)$ , and  $\delta \ll 1$ . In practical applications,  $\delta = \mathcal{O}(0.1)$  can be usually chosen for such a compliant robotic system. With (13), we can rewrite the SEA-driven robot dynamics as

$$\begin{aligned} M(q)\ddot{q} + C(q, \dot{q})\dot{q} + G(q) &= z + \tau_h \\ \delta^2\ddot{z} + \delta K_d \dot{z} + K_p z &= K_p(u_r - J\ddot{q}). \end{aligned} \quad (14)$$

The system (14) is singularly perturbed. The variables  $z$  and  $\dot{z}$  interpret “fast” variables and robot-level variables  $q$  and  $\dot{q}$  are “slow” variables. With  $\delta = 0$ , we can obtain

$$\bar{z} = \bar{u}_r - J\ddot{q} \quad (15)$$

where the overbars indicate the variables defined at  $\delta = 0$ . By substituting (15) into the robot-level dynamics in (14), one has

$$(M(\bar{q}) + J)\ddot{\bar{q}} + C(\bar{q}, \dot{\bar{q}})\dot{\bar{q}} + G(\bar{q}) = \bar{u}_r + \bar{\tau}_h. \quad (16)$$

Equation (16) is the *quasi-steady-state model*. From the Tikhonov theorem in [45], the following equations hold:

$$z = \bar{z} + \rho(\tau) + \mathcal{O}(\delta), \quad q = \bar{q} + \mathcal{O}(\delta) \quad (17)$$

where  $\tau = \frac{t}{\delta}$  is the fast time scale and  $\eta(\tau)$  satisfies the following *boundary layer dynamics*:

$$\frac{d^2\rho}{d\tau^2} + K_d \frac{d\rho}{d\tau} + K_p \rho = 0. \quad (18)$$

By choosing  $K_d$ , the *boundary layer dynamics* can be asymptotically stable and converge to the origin in a fast speed. It follows that the robot-level dynamics can be written up to  $\mathcal{O}(\delta)$  as

$$(M(q) + J)\ddot{q} + C(q, \dot{q})\dot{q} + G(q) = u_r + \tau_h + \rho\left(\frac{t}{\delta}\right). \quad (19)$$

Therefore, the following issue is designing a robot-level controller  $u_r$  for rehabilitation assistance.

### B. Robot-Level Control

With *fast-time* controller  $u_{\text{fast}}$ , the SEA-level dynamics can be stabilized in a fast time scale. In such a case, the *quasi-steady* dynamics is achieved, and the entire system dynamics can be treated as a reduced-order form. As  $\rho(\frac{t}{\delta})$  in (19) belongs to the fast time-scale variable and will rapidly converge to zero, it is ignored here for the convenience of control design. Now,

the reduced-order multijoint SEA-driven robot dynamics can be formulated in the common time scale as

$$(M(q) + J)\ddot{q} + C(q, \dot{q})\dot{q} + G(q) = u_r + \tau_h. \quad (20)$$

The AAN control law is developed according to the robot-level dynamics as the human–robot interaction directly drives robot-level dynamics. The entire control law can be constructed as follows:

$$\begin{cases} u_r = u_{\text{ref}} + u_{\text{learn}} + u_{\text{stable}} \\ u_{\text{ref}} = (M(q) + J)\ddot{q}_{\text{ref}} + C(q, \dot{q})\dot{q}_{\text{ref}} + G(q) \\ u_{\text{learn}} = K(t)e + D(t)\dot{e} + \tau(t) \\ u_{\text{stable}} = L_i e \end{cases} \quad (21)$$

where  $e = \dot{e} + \lambda e$  is a sliding vector composed of error vector and error velocity vector with a constant proportion  $\lambda$ .  $u_{\text{ref}}$  is a baseline control term for the realization of effective motion and  $\dot{q}_{\text{ref}}$  and  $\ddot{q}_{\text{ref}}$  are defined as

$$\dot{q}_{\text{ref}} = \dot{q}_d + \lambda e, \quad \ddot{q}_{\text{ref}} = \ddot{q}_d + \lambda \dot{e}. \quad (22)$$

$u_{\text{learn}}$  is an iterative learning control term, in which  $\tau(t)$  is a time-varying learned feedforward term and  $K(t)$  and  $D(t)$  are stiffness and damping matrixes learned through interaction with the trainee.  $u_{\text{stable}}$  is a robust term whose parameters are periodically updated according to human intention evaluation. It is assumed that there exist minimal required effort of stiffness  $K_m(t)$ , damping  $D_m(t)$ , and feedforward torque  $\tau_m(t)$  satisfying

$$\int_t^{t+T} -\{\varepsilon^T(\sigma) K_m(t)e(t) + \varepsilon^T(\sigma) D_m(t)\dot{e}(t) + \varepsilon^T(\sigma) \tau_m(t) + \varepsilon^T(\sigma) \tau_h(t)\} d\sigma \leq 0. \quad (23)$$

This assumption is set according to (3).

### C. Human–Robot Interaction Evaluation

In order to adjust the assistance level according to the trainee’s participation level and thus improve rehabilitation efficiency, the human–robot interaction will be evaluated first. In this article, the AAN method is implemented on a planar SEA-driven rehabilitation robot, so that the interaction force is measured and denoted as in two directions along the defined Cartesian coordinate in Fig. 2(b), which is also the coordinate of the human–robot motion space.

For better illustration of the evaluation process, a sketch is drawn as Fig. 4. For evaluating the robotic assistance process through the interaction force  $F_{\text{int}} = (F_x, F_y)$ , we decompose the interaction force vector as two orthogonal components: one is the along the tangential direction of the task motion (parallel to the reference velocity  $(\dot{x}_d, \dot{y}_d)$ ), and the other is along the normal direction of the task motion (parallel to the orthogonal vector of reference velocity). One of the orthogonal vectors of  $(\dot{x}_d, \dot{y}_d)$  is  $(-\dot{y}_d, \dot{x}_d)$ . It is also drawn in Fig. 4(b), which shows the decomposition principle. The force projection on the vector  $(\dot{x}_d, \dot{y}_d)$  can be computed as

$$F_{\text{int}}^{/\!/} = [F_x(t) \quad F_y(t)] \frac{[\dot{x}_d \quad \dot{y}_d]^T}{\sqrt{\dot{x}_d^2 + \dot{y}_d^2}} \quad (24)$$

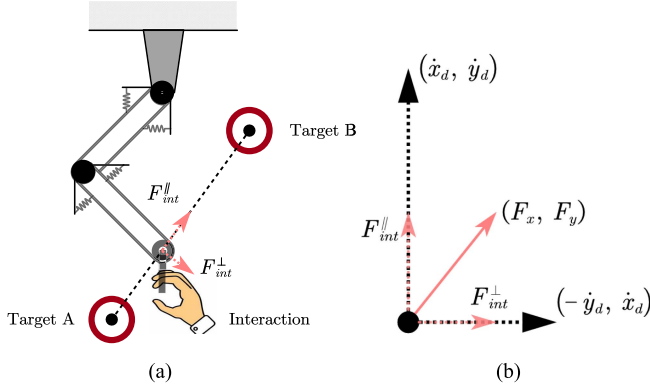


Fig. 4. Process of human–robot interaction evaluation. (a) Springs on the robotic joints symbolically show the compliance from the SEAs. (b) With the reference velocity direction, the interaction force vector is decomposed according to the principle of orthogonal decomposition.

and the force projection on the vector  $(-\dot{y}_d, \dot{x}_d)$  is

$$F_{\text{int}}^{\perp} = [ F_x(t) \ F_y(t) ] \frac{[ -\dot{y}_d \ \dot{x}_d ]^T}{\sqrt{\dot{x}_d^2 + \dot{y}_d^2}}. \quad (25)$$

According to the definitions above, positive  $F_{\text{int}}^{\parallel}$  means that the subject is pulling the robot along the reference moving direction and negative  $F_{\text{int}}^{\parallel}$  means that the subject is resisting the moving. Similarly, the value of  $F_{\text{int}}^{\perp}$  denotes the strength that subject exerted on the robot in the vertical direction of the reference motion. As we will use the absolute value to evaluate the interaction in normal direction, the sign of  $F_{\text{int}}^{\perp}$  will not affect the evaluation.

The evaluation force will not be constantly fed back to the control loop for assistance adaption. During the repetitive rehabilitation tasks, interaction force may suddenly increase because of unexpected conditions like pause, muscle spasm, etc. Therefore, constantly adjusting the assistance may not be a reliable way. In our study, the average interaction forces of each task iteration will be calculated in the two orthogonal directions. For the  $i$ th operation of the training task, the following tangential evaluation factor is defined:

$$r_i = \frac{1}{T} \int_{T_i}^{T_{i+1}} F_{\text{int}}^{\parallel} dt \quad (26)$$

where  $T$  is the task period and  $T_i$  and  $T_{i+1}$  denote the initial time of the  $i$ th and  $(i+1)$ th operation, respectively. Correspondingly, in the normal direction of the task motion, we define the following vertical evaluation factor:

$$r_i^{\text{vertical}} = \frac{1}{T} \int_{T_i}^{T_{i+1}} F_{\text{int}}^{\perp} dt. \quad (27)$$

The two evaluation factors  $r_i$  and  $r_i^{\text{vertical}}$  reflect the trainee's intention and participation level at desired moving direction and its vertical direction.

According to the evaluation principles above, high positive value of  $r_i$  means that the trainee tries to move faster than the robot or the expected speed. In such a case, the robot should reduce its control effort and allow larger motion error, so that

the trainee can get more freedom and be encouraged to improve the engagement during training. On the contrary, high negative value of  $r_i$  means that the trainee tries to move slower than the expected speed. The robot will increase the control effort to assist the trainee complete the training task better. However, when the absolute value of  $r_i$  is too high, the trainee is considered unable to operate the task in a satisfactory way. Then, the robot will also increase the assistance for guaranteeing the effective training and guidance. This is the main idea for encouraging participation of the trainee. In contrast, low value of  $|r_i|$  means that the trainee can excellently operate the desired task in the target direction. For the vertical evaluation factor  $r_i^{\text{vertical}}$ , high absolute value means that the trainee is trying to leave the target path in the vertical direction. This may cause failure of the training task, for example, a reaching task. The robot will iteratively correct the trainee's movement to the desired position, which is inspired from human-like learning way [31], so that effective training can be achieved.

#### D. Assistance Adaption

The assistance adaption is designed according to the human–robot evaluation results. The updating method for the robust term  $u_{\text{stable}}$  is designed with tangential evaluation factor  $r_i$ , so that the robot can efficiently change the stability region according to periodical evaluation. The updating law is

$$L_i = (1 + \eta_i) L_0, \quad \eta_i = (1 + \eta) (1 + \eta_{i-1}) - 1 \quad (28)$$

where  $\eta_0 = 0$ ,  $L_0$  is the initial robust gain, and  $\eta$  is the updating rate satisfying

$$\begin{cases} \eta = 0, & -r_{\min} \leq r_i \leq r_{\max} \\ -1 < \eta < 0, & r_{\min} < r_i \leq r_{\max} \\ 0 < \eta < 1, & -r_{\max} \leq r_i < -r_{\min} \\ \eta = 2, & |r_i| > r_{\max} \end{cases} \quad (29)$$

with the upper and lower bounds of  $|r_i|$ ,  $r_{\min}$ , and  $r_{\max}$ .

The impedance control parameters  $K(t)$ ,  $D(t)$ , and  $\tau(t)$  are designed with the learning algorithm and the vertical evaluation factor  $r_i^{\text{vertical}}$  as follows:

$$\begin{cases} \Delta K(t) = K(t) - K(t-T) = Q_K (\varepsilon e^T - (1 + \gamma_i) K(t)) \\ \Delta D(t) = D(t) - D(t-T) = Q_D (\varepsilon \dot{e}^T - (1 + \gamma_i) D(t)) \\ \Delta \tau(t) = \tau(t) - \tau(t-T) = Q_\tau (\varepsilon - (1 + \gamma_i) \tau(t)) \end{cases} \quad (30)$$

where  $\gamma_i \in (-1, 1)$  is the forgetting factor of the  $i$ th operation.  $Q_\tau$ ,  $Q_K$ , and  $Q_D$  are all symmetric positive-definite constant matrixes. During the first rehabilitation period, the learning results are all set to be zero, which means

$$\tau(t) = 0^{n \times 1}, K(t) = 0^{n \times n}, D(t) = 0^{n \times n}, \quad t \in [0, T]. \quad (31)$$

With the iterative learning method, the robot can gradually handle the interaction effects from the trainee's hand. The updating method for forgetting factor  $\gamma_i$  is defined as follows:

$$\gamma_i = (1 + \zeta) (1 + \gamma_{i-1}) - 1 \quad (32)$$

where  $\zeta$  is the updating rate satisfying

$$\begin{cases} \zeta = 0, & r_{\min}^{\text{vertical}} \leq |r_i^{\text{vertical}}| \leq r_{\max}^{\text{vertical}} \\ -1 < \zeta < 0, & |r_i^{\text{vertical}}| > r_{\max}^{\text{vertical}} \\ 0 < \zeta < 1, & |r_i^{\text{vertical}}| < r_{\min}^{\text{vertical}} \end{cases} \quad (33)$$

with the upper and lower bounds of  $|r_i^{\text{vertical}}|$ ,  $r_{\max}^{\text{vertical}}$ , and  $r_{\min}^{\text{vertical}}$ .

Clearly, with the above periodically updating method, the stable term  $u_{\text{stable}}$  and impedance learning term  $u_{\text{learn}}$  in (21) will directly affect the adaption of assistance in a composite way. Finally, the human–robot interaction evaluation-based AAN method introduced in Fig. 3 and (21) is achieved. With  $u_{\text{ref}}$  in (21), the robot can guarantee effective moving. For a given rehabilitation task in the form of motion trajectory,  $u_{\text{stable}}$  in (21) is periodically updated according to (28), and  $u_{\text{learn}}$  in (21) is updated according to (30) and (32). During the following stability analysis, we will explain how the iterative learning algorithm is derived and how the updating parameters affect the assistance level.

#### E. Stability Analysis of Human–Robot Interaction

According to (19) and (20), the stability of human–robot interaction system depends on the robot-level control  $u_r$ . It will be shown that under the proposed robot-level control scheme in (21) with adapting laws in (28), (32), and (30), the human–robot motion error  $\varepsilon$  will be limited in a bounded region. Besides, with the assumption in (23) and the impedance learning algorithm in (30), the impedance learning error will also be shown to be bounded.

For the stability analysis, the following Lyapunov-like cost functions are defined to be minimized:

$$\begin{aligned} V &= V_s + V_l \\ V_s &= \frac{1}{2} \varepsilon^T (M + J) \varepsilon \\ V_l &= \frac{1}{2} \int_{t-T}^t \tilde{\Phi}^T(\sigma) Q^{-1} \tilde{\Phi}(\sigma) d\sigma. \end{aligned} \quad (34)$$

In (34),  $\tilde{\Phi}(t)$  denotes the learning error vector and is defined as

$$\begin{aligned} \tilde{\Phi}(t) &= \Phi^*(t) - \Phi(t) \\ &= \left[ \text{vec}(\tilde{K}(t))^T, \text{vec}(\tilde{D}(t))^T, \tilde{\tau}(t)^T \right]^T \end{aligned} \quad (35)$$

with

$$\begin{aligned} \tilde{K}(t) &= K_m(t) - K(t) \\ \tilde{D}(t) &= D_m(t) - D(t) \\ \tilde{\tau}(t) &= \tau_m(t) - \tau(t) \end{aligned} \quad (36)$$

and

$$\begin{aligned} \Phi^*(t) &= \left[ \text{vec}(K_m(t))^T, \text{vec}(D_m(t))^T, \tau_m^T(t) \right]^T \\ \Phi(t) &= \left[ \text{vec}(K(t))^T, \text{vec}(D(t))^T, \tau^T(t) \right]^T \\ Q &= \text{diag}(I \otimes Q_K, I \otimes Q_D, Q_\tau) \end{aligned} \quad (37)$$

where  $\text{vec}(\cdot)$  is the column vectorization operator.

Instead of making the cost function not increase all the time like strict Lyapunov stability showing, we will drive them stable during each period and keep them in a stability region, which can be tuned by the updating parameters  $L_i$  and  $\gamma_i$ . This means when the updating parameters stay the same, the stable motion is defined as

$$\Delta V = V(t) - V(t-T) \leq 0. \quad (38)$$

First, by differentiating  $V_s$ , one has

$$\begin{aligned} \dot{V}_s &= \varepsilon^T (M + J) \dot{\varepsilon} + \varepsilon^T C \varepsilon \\ &= \varepsilon^T [(M + J) \ddot{q}_{\text{ref}} + C \dot{q}_{\text{ref}} + G - \bar{u} - \tau_h] \\ &= -\varepsilon^T L_i \varepsilon - \varepsilon^T \tau - \varepsilon^T K(t) e - \varepsilon^T D(t) \dot{e} - \varepsilon^T \tau_h. \end{aligned} \quad (39)$$

According to (23), the following inequality can be derived:

$$\begin{aligned} \Delta V_s &= V_s(t) - V_s(t-T) \\ &= \int_{t-T}^t \left\{ -\varepsilon^T \min(L_i, L_{i-1}) \varepsilon - \varepsilon^T \tau(\sigma) \right. \\ &\quad \left. - \varepsilon^T K(\sigma) e - \varepsilon^T D(\sigma) \dot{e} - \varepsilon^T \tau_h \right\} d\sigma \\ &\leq \int_{t-T}^t \left\{ -\varepsilon^T \min(L_i, L_{i-1}) \varepsilon - \varepsilon^T \tilde{\tau}(\sigma) \right. \\ &\quad \left. - \varepsilon^T \tilde{K}(\sigma) e - \varepsilon^T \tilde{D}(\sigma) \dot{e} \right\} d\sigma. \end{aligned} \quad (40)$$

According to the definition of  $\tilde{\Phi}$  and  $Q$ , one has

$$\Delta V_l = V_l(t) - V_l(t-T)$$

$$\begin{aligned} &= \frac{1}{2} \int_{t-T}^t \left\{ \text{tr} \left\{ \tilde{K}^T(\sigma) Q_K^{-1} \tilde{K}(\sigma) \right. \right. \\ &\quad \left. \left. - \tilde{K}^T(\sigma-T) Q_K^{-1} \tilde{K}(\sigma-T) \right\} \right. \\ &\quad \left. + \text{tr} \left\{ \tilde{D}^T(\sigma) Q_D^{-1} \tilde{D}(\sigma) - \tilde{D}^T(\sigma-T) Q_D^{-1} \tilde{D}(\sigma-T) \right\} \right. \\ &\quad \left. + \tilde{\tau}^T(\sigma) Q_\tau^{-1} \tilde{\tau}(\sigma) - \tilde{\tau}^T(\sigma-T) Q_\tau^{-1} \tilde{\tau}(\sigma-T) \right\} d\sigma. \end{aligned} \quad (41)$$

By rewriting (30) as

$$\begin{aligned} \Delta \tilde{K}(t) &= Q_K (\varepsilon e^T - (1 + \gamma_i) K(t)) \\ \Delta \tilde{D}(t) &= Q_D (\varepsilon \dot{e}^T - (1 + \gamma_i) D(t)) \\ \Delta \tilde{\tau}(t) &= Q_\tau (\varepsilon - (1 + \gamma_i) \tau(t)) \end{aligned} \quad (42)$$

with the periodic property of  $K_m(t)$ ,  $D_m(t)$ , and  $\tau_m(t)$ , one can get the following equality with the first term in the integrand of (41):

$$\begin{aligned} &\text{tr} \left\{ \tilde{K}^T(\sigma) Q_K^{-1} \tilde{K}(\sigma) - \tilde{K}^T(\sigma-T) Q_K^{-1} \tilde{K}(\sigma-T) \right\} \\ &= \text{tr} \left\{ \left( \tilde{K}^T(\sigma) - \tilde{K}^T(\sigma-T) \right) Q_K^{-1} \left( \tilde{K}(\sigma) + \tilde{K}(\sigma-T) \right) \right\} \\ &= \text{tr} \left\{ \left( \tilde{K}^T(\sigma) - \tilde{K}^T(\sigma-T) \right) Q_K^{-1} \left( \tilde{K}(\sigma) + \tilde{K}(\sigma-T) \right) \right\} \\ &= -\text{tr} \left\{ \Delta K^T(\sigma) Q_K^{-1} \Delta K^T(\sigma) \right\} + 2 \text{tr} \left\{ \Delta K^T(\sigma) Q_K^{-1} \tilde{K}(\sigma) \right\} \end{aligned}$$

$$= -\text{tr} \{ \Delta K^T(\sigma) Q_K^{-1} \Delta K^T(\sigma) \} + 2\varepsilon^T \tilde{K}(\sigma) e \\ - 2(1 + \gamma_i) \text{tr} \{ K^T(\sigma) \tilde{K}(\sigma) \}. \quad (43)$$

Using similar derivation, one has

$$\text{tr} \{ \tilde{D}^T(\sigma) Q_D^{-1} \tilde{D}(\sigma) - \tilde{D}^T(\sigma - T) Q_D^{-1} \tilde{D}(\sigma - T) \} \\ = -\text{tr} \{ \Delta \tilde{D}^T(\sigma) Q_D^{-1} \Delta \tilde{D}^T(\sigma) \} + 2\varepsilon^T \tilde{D}(\sigma) \dot{e} \\ - 2(1 + \gamma_i) \text{tr} \{ D^T(\sigma) \tilde{D}(\sigma) \} \quad (44)$$

and

$$\text{tr} \{ \tilde{\tau}^T(\sigma) Q_\tau^{-1} \tilde{\tau}(\sigma) - \tilde{\tau}^T(\sigma - T) Q_\tau^{-1} \tilde{\tau}(\sigma - T) \} \\ = -\text{tr} \{ \Delta \tilde{\tau}^T(\sigma) Q_\tau^{-1} \Delta \tilde{\tau}^T(\sigma) \} + 2\varepsilon^T \tilde{\tau}(\sigma) \\ - 2(1 + \gamma_i) \text{tr} \{ \tau^T(\sigma) \tilde{\tau}(\sigma) \}. \quad (45)$$

By incorporating (43)–(45) into (41), one can finally get

$$\Delta V_l = -\frac{1}{2} \int_{t-T}^t \Delta \tilde{\Phi}^T(\sigma) Q^{-1} \Delta \tilde{\Phi}(\sigma) d\sigma \\ - \int_{t-T}^t \gamma_i \tilde{\Phi}^T(\sigma) \tilde{\Phi}(\sigma) d\sigma \\ + \int_{t-T}^t \{ \varepsilon^T \tilde{K}(\sigma) e + \varepsilon^T \tilde{D}(\sigma) \dot{e} + \varepsilon^T \tilde{\tau}(\sigma) \} d\sigma. \quad (46)$$

By combining with (40), one further has

$$\Delta V = \Delta V_s + \Delta V_l \\ \leq -\frac{1}{2} \int_{t-T}^t \{ \Delta \tilde{\Phi}^T(\sigma) Q^{-1} \Delta \tilde{\Phi}(\sigma) + \varepsilon^T \min(L_{i-1}, L_i) \varepsilon \} d\sigma \\ - \int_{t-T}^t \gamma_i \{ \tilde{\Phi}^T(\sigma) \tilde{\Phi}(\sigma) + \tilde{\Phi}^T(\sigma) \Phi^*(\sigma) \} d\sigma. \quad (47)$$

A sufficient condition to make  $\Delta V$  nonpositive is

$$\varepsilon^T \min(L_{i-1}, L_i) \varepsilon + \gamma_i \tilde{\Phi}^T \tilde{\Phi} + \gamma_i \tilde{\Phi}^T \Phi^* \\ \geq \lambda_L \|\varepsilon\|^2 + \gamma_i \|\tilde{\Phi}\|^2 - \gamma_i \|\tilde{\Phi}\| \|\Phi^*\| \geq 0 \quad (48)$$

where  $\lambda_L$  is the smallest eigenvalue of  $L_{i-1}$  and  $L_i$ , and  $\|\Phi^*\|$  and  $\|\tilde{\Phi}\|$  are the Euclidean norms of the required minimum learning terms and errors. According to this condition, the stability region and the learning process of the human–robot system can be adjusted by tuning  $L_i$  and  $\gamma_i$ . More precisely, the motion error can be limited by the following relation:

$$\|\varepsilon\|^2 = \frac{\gamma_i}{\lambda_L} (\|\tilde{\Phi}\| - \|\Phi^*\|) \|\tilde{\Phi}\|. \quad (49)$$

Therefore, increasing  $\lambda_L$  will improve the moving accuracy and robustness, and decreasing  $\lambda_L$  will enlarge the allowable motion error.

#### IV. EXPERIMENTAL EVALUATION

The proposed human–robot interaction evaluation-based AAN method was implemented on a two-DOF SEA-driven

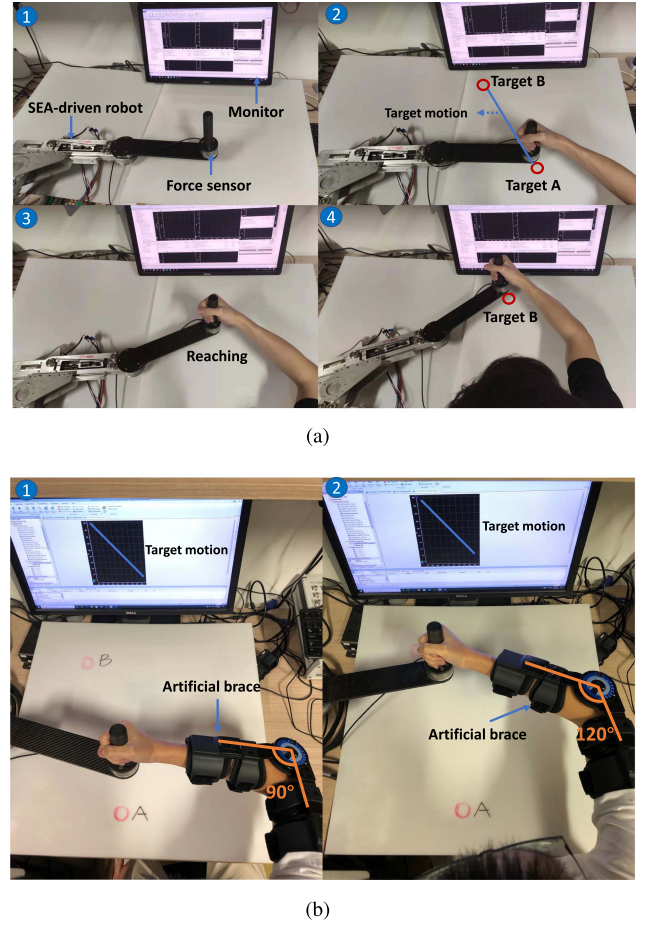


Fig. 5. Experiment setup and process. (a) Subject will hold the handle and move with the assistance from the robot. The force sensor at the end-effector will measure and feedback the human–robot interactive force to the controller. The target points and motion are demonstrated with red circles and a blue straight line. (b) In order to simulate the motion limitation of the impaired upper limb, an artificial brace is utilized for limiting a healthy subject’s motion, in which the motion range is 90–120°.

rehabilitation robot, as shown in Fig. 2. This section introduces the experiments and validation results.

#### A. Experimental Setup

The rehabilitation training motion is defined as a reaching task with constant moving speed between two target points, which is a typical training movement for rehabilitation. The experimental setup and the process of reaching are shown in Fig. 5(a), and the red circles denote two target points A and B, which are also shown in Fig. 4. During the training process, the trainee will repeat the reaching movements between the two points. The end-effector of the SEA-driven robot is equipped with a force sensor, which sits under the handle. The trainee will grasp and hold the handle to receive the robotic assistance. Human–robot interactive forces are measured by the force sensor and fed back to dSPACE control board for real-time control. All the data from sensors or control algorithm will be collected by dSPACE I/O board and can be displayed on the PC with customized software ControlDesk. As shown in Fig. 5(b), the target motion trajectory is shown on the screen.

During our experiments, two conditions are considered, and corresponding experiments are conducted. In condition 1, a healthy subject was asked to operate the rehabilitation tasks with different participation levels. For verifying the effectiveness and feasibility of the proposed AAN method, the experiments were conducted in three cases involving different human participation levels and participation-changing process. In condition 2, we utilize an upper limb brace to artificially exert motion limitations to the subject's elbow joint, which is shown in Fig. 5(b). We try to simulate the motion limitations of the impaired limb of the patient. In such a way, we can test the practical potentials of the SEA-driven robot and the proposed AAN method in clinical applications. In our study, eight healthy subjects were involved.

*1) Experiments With One Healthy Subject Exerting Different Participation Levels:* For the convenience of testing, three participation levels of the trainee are defined first, which are passive level, positive level, and active level [46]. Passive level means that the trainee cannot provide any muscle strength during rehabilitation, and the robot should provide enough assistance to help finish the task. Positive level means that the trainee can provide partial or enough strength to finish the task and the robot only needs to provide necessary assistance. Active level means that the trainee can independently finish the rehabilitation task, and at the same time, he/she wants to speed up his movements [28]. Active level leads to stronger interaction, and the robot should further decrease the assistance and allow larger stability region (allowable error) so that the trainee gets more freedom. The experiments were conducted in the following three cases.

*Case I—Passive rehabilitation for validation of learning process and motion correction:* The subject was asked to hold the handlebar and passively follow the moving of the robot without applying any active force. In this case, the interaction forces of task direction and its vertical direction would be both relatively large. We aimed to test if the iterative learning algorithm and periodic updating of  $\eta_i$  and  $\gamma_i$  can improve the motion performance periodically.

*Case II—Positive rehabilitation with vertical perturbation for validation of the learning strength updating:* The subject was asked to follow the robot motion positively so that the interaction force in the task direction would be small and the updating rate  $\gamma_i$  would not be increased. Simultaneously, perturbation force in the vertical direction was added artificially. We aimed to test if the forgetting factor  $\eta_i$  of the learning algorithm would be adjusted according to the vertical evaluation results and correct the reaching process.

*Case III—Multiple switching of the participation levels for validation of the entire AAN method:* The subject was asked to perform multiple switching of his/her participation levels during the rehabilitation. The switching process was passive to positive, positive to active, active to positive, positive to passive, and then stop. In this case, we aimed to test the adaption process of the AAN method and its potential for practical rehabilitation applications.

*2) Experiments With Simulated Upper Limb Impairments:* For simulating the impaired upper limb, we utilize an artificial brace to limit the healthy subjects' joint motion between  $90^\circ$  and  $120^\circ$ , as shown in Fig. 5(b). In this case, we aimed to test the

TABLE II  
PARTICIPANT CHARACTERISTICS

Participant	Sex	Age (years)	Mass (kg)	Height (m)
Subject 1	Male	30	67.0	1.83
Subject 2	Female	27	46.5	1.62
Subject 3	Male	28	86.3	1.70
Subject 4	Male	29	62.1	1.68
Subject 5	Male	26	75.5	1.82
Subject 6	Male	28	64.3	1.70
Subject 7	Male	24	70.0	1.73
Subject 8	Male	31	75.5	1.73

feasibility and effectiveness of the proposed AAN method for different subjects.

Eight healthy people were recruited for this study (age:  $27.9 \pm 2.2$  years; weight:  $68.4 \pm 11.7$  kg; and height:  $1.73 \pm 0.07$  m). All the subjects were required to provide voluntary effort as little as possible. The reaching process were repeated 20–30 times during each trial. Participant characteristics are detailed in Table II. Subjects gave informed consent, and testing was approved by the National University of Singapore Institutional Review Board (NUS-IRB-2022-216).

## B. Results and Discussion

During the implementation of the proposed AAN control method, the control parameter  $k_{\text{fast}}$  is chosen according to the analysis in Section III-A, especially (13) and (18). With necessary experimental tuning trials, the final value is set to be  $k_{\text{fast}} = 0.2$ . For the robust control term  $u_{\text{stable}}$  and learning control term  $u_{\text{learn}}$ , the factor  $\lambda$  defined in (22) is set to be 10. The initial value of the control gain of  $u_{\text{stable}}$  is set as  $L_0 = \text{diag}\{2, 2\}$ , which is relatively small for exciting sufficient iterative process. By setting  $r_{\min} = 1$  and  $r_{\max} = 3$ , the updating coefficient  $\eta$  for  $u_{\text{stable}}$  is obtained by

$$\begin{cases} \eta = 0, & -1 \leq r_i \leq 1 \\ \eta = -0.2, & 1 < r_i \leq 3 \\ \eta = 0.2, & -3 \leq r_i < -1 \\ \eta = 2, & |r_i| > 3 \end{cases}. \quad (50)$$

For the learning control term  $u_{\text{learn}}$ , the learning rate factors are selected as  $Q_K = \text{diag}\{50, 50\}$ ,  $Q_D = \text{diag}\{10, 10\}$ , and  $Q_\tau = \text{diag}\{20, 20\}$ . By setting  $r_{\min}^{\text{vertical}} = 0.1$  and  $r_{\max}^{\text{vertical}} = 0.5$ , the updating coefficient  $\zeta$  for  $u_{\text{learn}}$  is obtained by

$$\begin{cases} \zeta = 0, & 0.1 \leq |r_i^{\text{vertical}}| \leq 0.5 \\ \zeta = -0.2, & |r_i^{\text{vertical}}| > 0.5 \\ \zeta = 0.2, & |r_i^{\text{vertical}}| < 0.1 \end{cases}. \quad (51)$$

For comparison and demonstration, the root-mean-square error (RMSE) of Cartesian space is calculated as

$$\text{RMSE} = \frac{1}{H} \int_{t_0}^{t_0+H} \sqrt{(x_d - x)^2 + (y_d - y)^2} dt \quad (52)$$

where  $H$  is the considered duration. For further demonstration of the assistance level, the energy cost of the SEA-driven robot

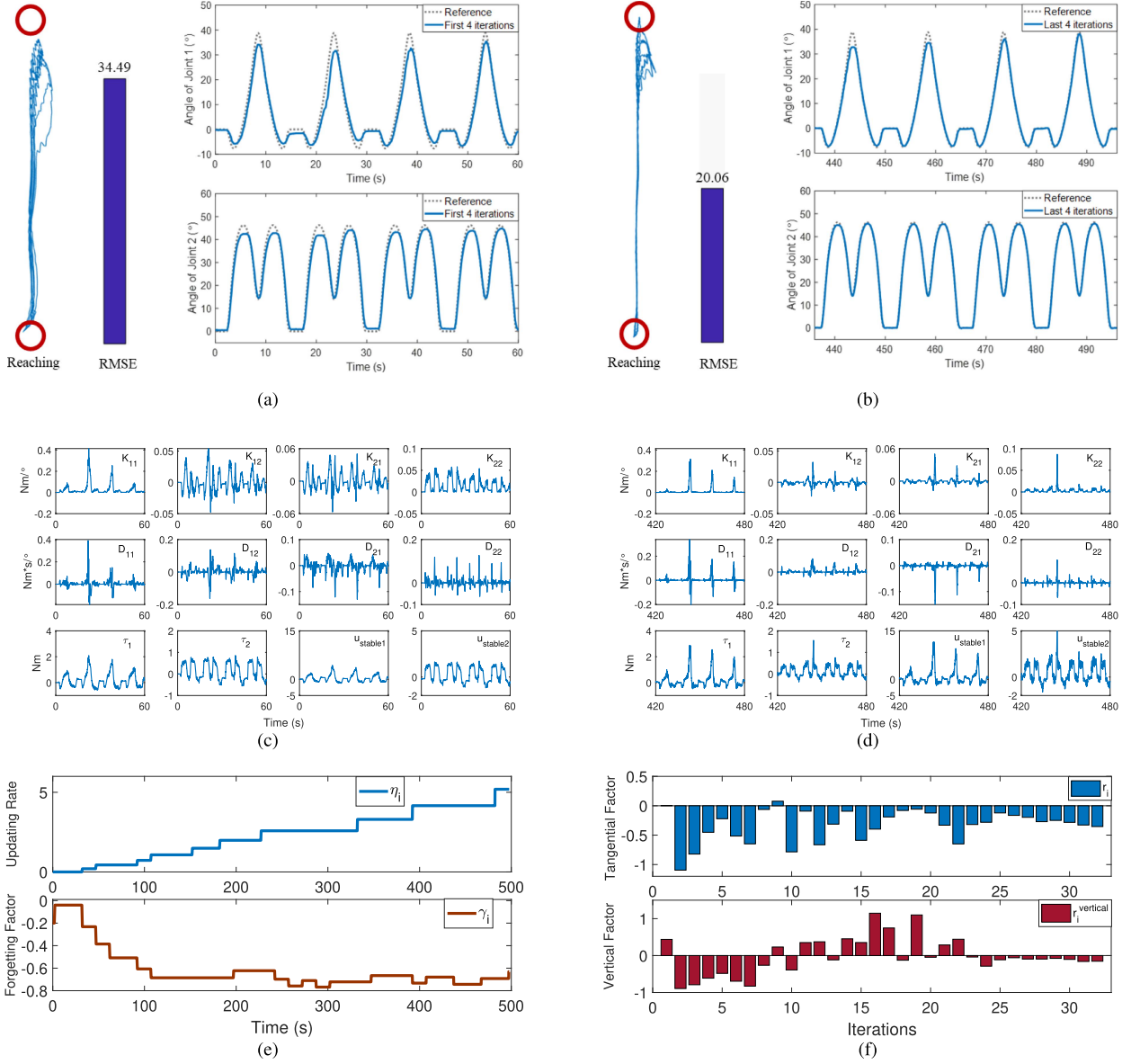


Fig. 6. Rehabilitation with passive-level participation. (a) First four iterations of the task, in which red circle denote two reaching targets and the barchart means RMSE (mm) of Cartesian space. (b) Last four iterations of the task. (c) Impedance parameters, feedforward torques, and stable term of the first four iterations. (d) Impedance parameters, feedforward torques, and stable term of the last four iterations. (e) Updating process of the coefficients, which include the updating factor  $\eta_i$  for the robust control term  $u_{\text{stable}}$  and forgetting factor  $\gamma_i$  for the learning control term  $u_{\text{learn}}$ . (f) Evaluation results of human–robot interaction with force measurement, which include the tangential evaluation factor  $r_i$  and the vertical evaluation factor  $r_i^{\text{vertical}}$ .

in each task is calculated as follows:

$$J_i = \int_{T_{i-1}}^{T_i} (u_1^2 + u_2^2) dt. \quad (53)$$

1) *Experiments With One Healthy Subject Exerting Different Participation Levels: Case I*—In this case, the subject was asked to perform the reaching task for 32 times. To show the performance of the AAN strategy when the subject passively moves, we compare the motion performance of the first four and the last four operations. The results are drawn as Fig. 6. As shown in Fig. 6(a) and (b), the performance of the last four operations is much better than that of the first four operations. Both of the reaching accuracy and straightness got gradually improved by operations. The Cartesian-space RMSE of these two groups

are 34.49 and 20.06 mm. From the joint-space trajectories in Fig. 6(a) and (b), it can be more clearly observed that the motion accuracy got improved with the increase of operating times. As the subject was passively performing the rehabilitation task, the human–robot interaction was relatively large and the robot needed to enhance the assistance level for bettering reaching. Fig. 6(c) and (d) shows the impedance parameters, feedforward torques, and stable term during the first four operations and the last four operations. Fig. 6(e) and (f) shows the parameters updating and human–robot interaction evaluation results during each operation.  $L_i$  was periodically increased to improve the reaching accuracy, and Fig. 6(f) shows that the tangential evaluation factor was in a high level for most of the rehabilitation time.  $\gamma_i$  decreased to a very low level as the vertical interaction

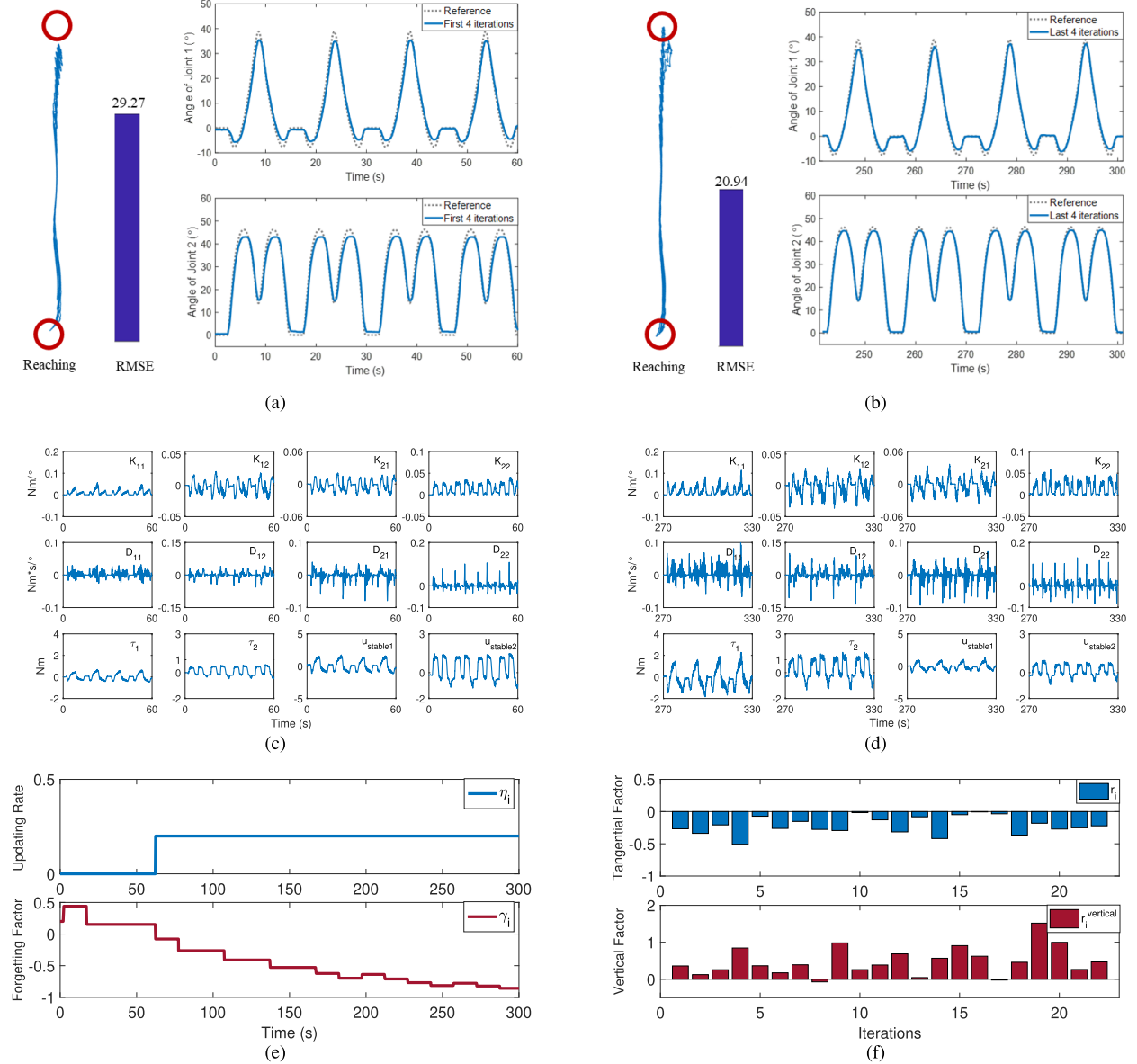


Fig. 7. Rehabilitation with positive-level participation and vertical perturbations. (a) First four iterations of the task, in which red circle denote two reaching targets and the barchart means RMSE (mm) of Cartesian space. (b) Last four iterations of the task. (c) Impedance parameters, feedforward torques, and stable term of the first four iterations. (d) Impedance parameters, feedforward torques, and stable term of the last four iterations. (e) Updating process of the coefficients that include the updating factor  $\eta_i$  for the robust control term  $u_{stable}$  and forgetting factor  $\gamma_i$  for the learning control term  $u_{learn}$ . (f) Evaluation results of human–robot interaction with force measurement, which include the tangential evaluation factor  $r_i$  and the vertical evaluation factor  $r_i^{vertical}$ .

was high as well, which can be observed from Fig. 6(f). As a result, it can be observed from Fig. 6(c) and (d) that robust term got increased. Although  $\gamma_i$  decreased,  $u_{learn}$  did not show increase. The main reason is that increasing  $u_{stable}$  decreases the motion error. This further indicates that smaller stable region will make the human–robot system robuster and less sensitive to interaction forces. For passive rehabilitation, this will lead to a good guidance.

*Case II*—In this case, the subject was asked to artificially add vertical perturbations, and the reaching task was performed for 20 times. Similar to the results in Case I, we draw the performance of the first four and the last four operations in Fig. 7. From Fig. 7(a) and (b), the reaching performance got gradually improved with the increase of operations. The Cartesian-space

RMSE was decreased by 7.33 mm, and the joint-space trajectories show the improvement as well. From Fig. 7(e) and (f),  $\eta_i$  was only increased by one time as in the tangential direction of the task, the subject could perform the rehabilitation task well. However, as the vertical interaction was large, the learning process was enhanced by increasing  $\gamma_i$ . From Fig. 7(c) and (d), it can be observed that the impedance learning process was clearly enhanced and correct the reaching movement. The stable term was partially decreased because of the decreasing motion error.

*Case III*—In this case, the subject was asked to change his/her participation level as introduced in the experimental setup. The experimental results are shown in Fig. 8. During each participation level, Fig. 8(a) still shows the first and the last four operations. It can be observed that if the subject passively participates

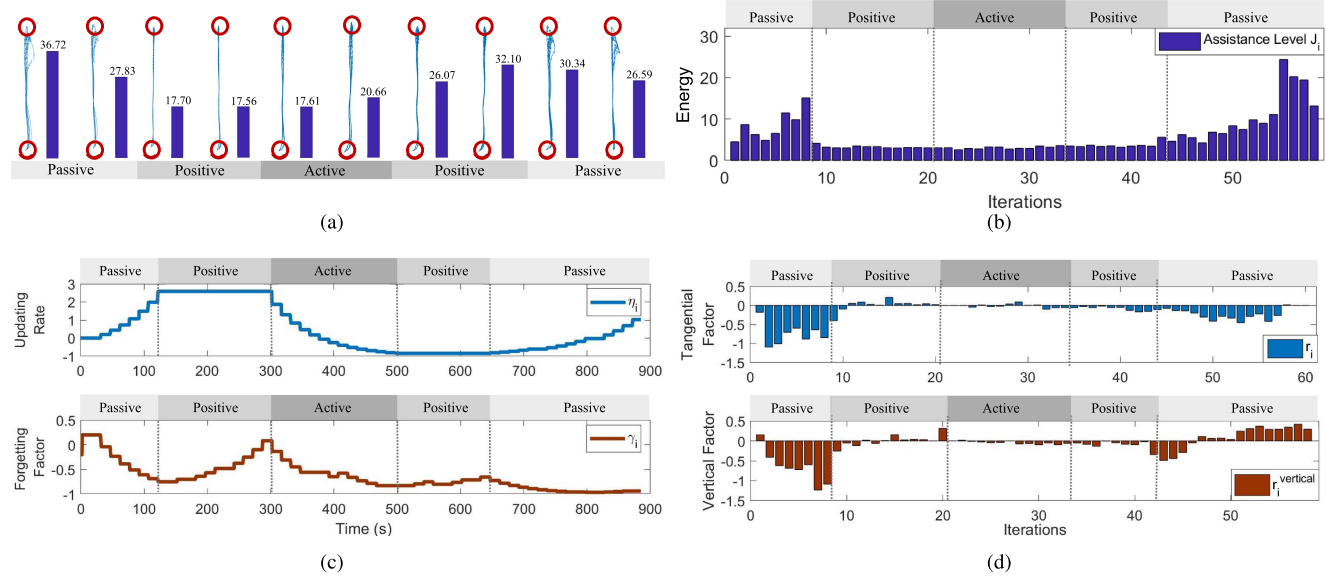


Fig. 8. Rehabilitation with multilevel participation change. (a) Reaching performance with different participation level. During each level, the red circles and blue lines denote the reaching process, and the blue strips denote the RMSE (mm) of the reaching process. The performance of the first four iterations and last iterations are drawn in order during each participation level. (b) Energy cost of the rehabilitation robot during each iteration. (c) Updating process of the coefficients, which include the updating factor  $\eta_i$  for the robust control term  $u_{\text{stable}}$  and forgetting factor  $\gamma_i$  for the learning control term  $u_{\text{learn}}$ . (d) Evaluation results of human–robot interaction with force measurement, which include the tangential evaluation factor  $r_i$  and the vertical evaluation factor  $r_i^{\text{vertical}}$ .

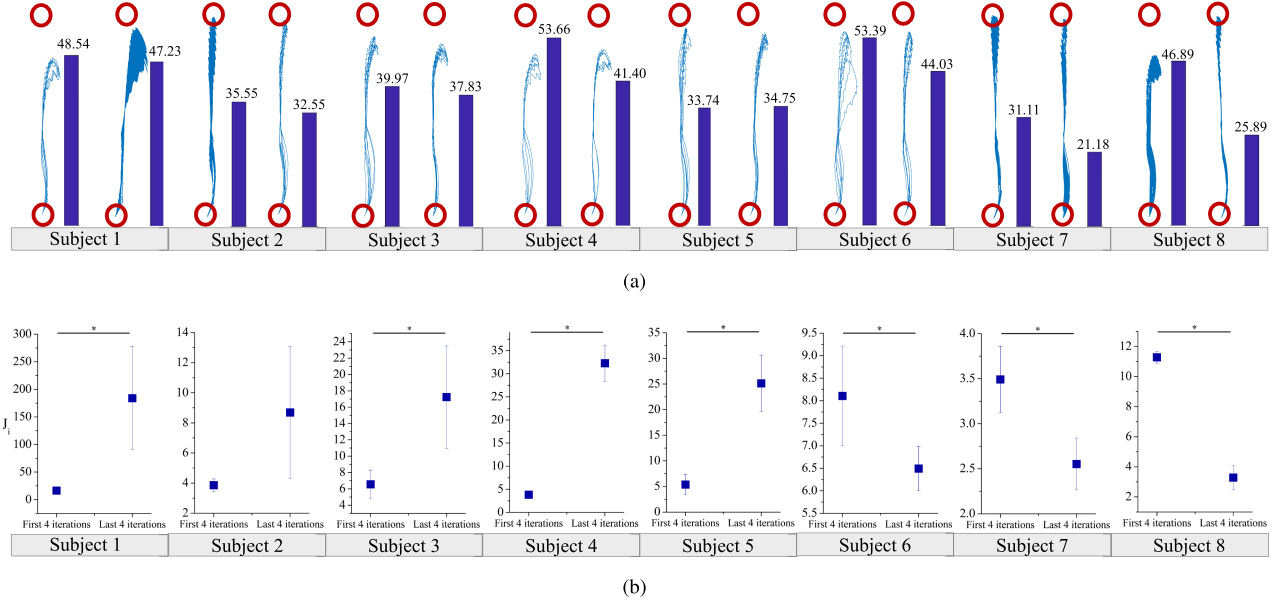


Fig. 9. Reaching performance of eight subjects with simulated impaired upper limb. (a) For each subject, the results of the first four iterations and the last four iterations are shown in left and right sides of the subfigure, respectively. The red circles and blue lines denote the reaching process, and the blue strips denote the RMSE (mm) of the reaching process. (b) Statistical results (mean  $\pm$  standard deviation) labeled with mean values of the robot effort during the first four iterations and last four iterations. The symbol “\*” denotes significant difference between two variables with  $p < 0.05$ .

the rehabilitation, the robot will always enhance the assistance to improve the motion performance by increasing  $\eta_i$  and decreasing  $\gamma_i$ , which are shown in Fig. 8(c). When the subject increased his participation and tried to positively move with the rehabilitation robot,  $L_i$  stopped periodic updating because the subject did not need more assistance. Simultaneously,  $\gamma_i$  was increased to reduce the learning strength. The rehabilitation performance

during positive level did not experience much change as the subject can almost independently accomplish the reaching task. When the subject further improved his participation to the active level,  $L_i$  got decreased to allow larger motion error so that the subject could obtain more active motion freedom. This is shown by the increased motion error in active-level duration in Fig. 8(a). However, the learning strength was increased by

decreasing  $\gamma_i$  as the vertical interaction got increased. During the following operations, similar conclusion can be summarized as well. For further demonstration, Fig. 8(b) shows the energy cost defined in (53). Obviously, the robot provided much larger assistance during passive participation level, and the AAN target was achieved with periodic updating of the parameters.

### 2) Experiments With Simulated Upper Limb Impairments:

During the experiments, the subjects were asked not to intentionally overcome the limitations from the brace and not to actively follow the motion of the robot. From the experimental results of Fig. 9(a), most of the subjects (except subject 5) achieved better reaching performance after some iterations. Fig. 9(b) gives statistical results of the robot effort, which is calculated according to (53). For comparing the changing of the robot effort generated by the proposed AAN controller, statistical significance was assessed using one-way analysis of variance and means comparison between the first four iterations and last four iterations used Tukey's test with significance level set at  $p < 0.05$ . It can be observed that, for Subjects 1–4, the decrease of the motion error is accompanied by the increase of the robot effort. For Subject 5, the reaching performance is relatively satisfactory and was not improved during the iterations. However, the robot effort for assisting Subject 5 was increased during the training. The main reason is that Subject 5 exerted uncertain interactive forces to the robot, and the artificial impairment did not fit him well. For Subjects 6–8, the reaching performance got obviously improved after some iterations. However, the robot effort got decreased. The main reason is that the subjects provided partial voluntary efforts to follow the robot after understanding the target motion. This caused the decrease of human–robot interactive forces and the iterative decrease of robot effort. To some extent, Subjects 6–8 showed active participation during the experiments.

Overall, all the participants could finish the experiments without much difficulty, and the SEA-driven robot did not show any instability under the proposed controller. The experimental results with artificial impairments demonstrate that the proposed AAN method can iteratively increase the robot effort when needed. If the human provides more voluntary effort and actively increases the motion performance, the robot will decrease the assistance. In such a way, the AAN principle can be realized.

## V. CONCLUSION

In this article, a human–robot interaction evaluation-based AAN method was proposed to perform upper limb rehabilitation with the multijoint SEA-driven robot. The SEA-level dynamics was first stabilized by the singular perturbation approach, which leads to a fast-time controller. Then, considering the uncertain human–robot interaction and changing participation level, an assistance adaption idea was realized with periodical human–robot interaction evaluation. During adaption method, the iterative learning algorithm was adopted to derive a learning control term for compliantly handling the human–robot interaction effects. The assistance provided by the robot was adjusted periodically, so that the human participation can be promoted. The proposed AAN method was validated with implementations

on a two-DOF SEA-driven robot. It can be directly applied to upper limb rehabilitation under different tasks and with other compliant rehabilitation robots. During further research, we will test this method on more subjects for evaluation and develop new rehabilitation robot for practical clinical trials.

## ACKNOWLEDGMENT

Shaishuai Han would like to thank the China Scholarship Council for supporting his visiting in Singapore.

## REFERENCES

- [1] R. Riener, T. Nef, and G. Colombo, "Robot-aided neurorehabilitation of the upper extremities," *Med. Biol. Eng. Comput.*, vol. 43, no. 1, pp. 2–10, 2005.
- [2] H. I. Krebs, N. Hogan, M. L. Aisen, and B. T. Volpe, "Robot-aided neurorehabilitation," *IEEE Trans. Rehabil. Eng.*, vol. 6, no. 1, pp. 75–87, Mar. 1998.
- [3] R. Riener, L. Lunenburger, S. Jezernik, M. Anderschitz, G. Colombo, and V. Dietz, "Patient-cooperative strategies for robot-aided treadmill training: First experimental results," *IEEE Trans. Neural Syst. Rehabil. Eng.*, vol. 13, no. 3, pp. 380–394, Sep. 2005.
- [4] P. Maciejasz, J. Eschweiler, K. Gerlach-Hahn, A. Jansen-Troy, and S. Leonhardt, "A survey on robotic devices for upper limb rehabilitation," *J. Neuroeng. Rehabil.*, vol. 11, no. 1, pp. 1–29, 2014.
- [5] H. I. Krebs et al., "Robot-aided neurorehabilitation: A robot for wrist rehabilitation," *IEEE Trans. Neural Syst. Rehabil. Eng.*, vol. 15, no. 3, pp. 327–335, Sep. 2007.
- [6] N. Vitiello et al., "NEUROExos: A powered elbow exoskeleton for physical rehabilitation," *IEEE Trans. Robot.*, vol. 29, no. 1, pp. 220–235, Feb. 2013.
- [7] Z. Li, C.-Y. Su, L. Wang, Z. Chen, and T. Chai, "Nonlinear disturbance observer-based control design for a robotic exoskeleton incorporating fuzzy approximation," *IEEE Trans. Ind. Electron.*, vol. 62, no. 9, pp. 5763–5775, Sep. 2015.
- [8] R. v. Ham, T. Sugar, B. Vanderborght, K. Hollander, and D. Lefebvre, "Compliant actuator designs," *IEEE Robot. Autom. Mag.*, vol. 3, no. 16, pp. 81–94, Sep. 2009.
- [9] H. Yu, S. Huang, G. Chen, Y. Pan, and Z. Guo, "Human–robot interaction control of rehabilitation robots with series elastic actuators," *IEEE Trans. Robot.*, vol. 31, no. 5, pp. 1089–1100, Oct. 2015.
- [10] J. F. Veneman, R. Kruidhof, E. E. G. Hekman, R. Ekkelenkamp, E. H. F. Van Asseldonk, and H. Van Der Kooij, "Design and evaluation of the LOPES exoskeleton robot for interactive gait rehabilitation," *IEEE Trans. Neural Syst. Rehabil. Eng.*, vol. 15, no. 3, pp. 379–386, Sep. 2007.
- [11] T. Chen, R. Casas, and P. S. Lum, "An elbow exoskeleton for upper limb rehabilitation with series elastic actuator and cable-driven differential," *IEEE Trans. Robot.*, vol. 35, no. 6, pp. 1464–1474, Dec. 2019.
- [12] X. Li, Y.-H. Liu, and H. Yu, "Iterative learning impedance control for rehabilitation robots driven by series elastic actuators," *Automatica*, vol. 90, pp. 1–7, 2018.
- [13] A. Calanca and P. Fiorini, "A rationale for acceleration feedback in force control of series elastic actuators," *IEEE Trans. Robot.*, vol. 34, no. 1, pp. 48–61, Feb. 2018.
- [14] D. Kim, K. Koh, G.-R. Cho, and L.-Q. Zhang, "A robust impedance controller design for series elastic actuators using the singular perturbation theory," *IEEE/ASME Trans. Mechatron.*, vol. 25, no. 1, pp. 164–174, Feb. 2020.
- [15] G. Aguirre-Ollinger and H. Yu, "Lower-limb exoskeleton with variable-structure series elastic actuators: Phase-synchronized force control for gait asymmetry correction," *IEEE Trans. Robot.*, vol. 37, no. 3, pp. 763–779, Jun. 2021.
- [16] W. Huo, M. A. Alouane, Y. Amarat, and S. Mohammed, "Force control of SEA-based exoskeletons for multimode human–robot interactions," *IEEE Trans. Robot.*, vol. 36, no. 2, pp. 570–577, Apr. 2020.
- [17] M. Keppler, D. Lakatos, C. Ott, and A. Albu-Schäffer, "Elastic structure preserving (ESP) control for compliantly actuated robots," *IEEE Trans. Robot.*, vol. 34, no. 2, pp. 317–335, Apr. 2018.
- [18] A. U. Pehlivian, D. P. Losey, and M. K. O'Malley, "Minimal assist-as-needed controller for upper limb robotic rehabilitation," *IEEE Trans. Robot.*, vol. 32, no. 1, pp. 113–124, Feb. 2016.

- [19] M. Menner, L. Neuner, L. Lünenburger, and M. N. Zeilinger, "Using human ratings for feedback control: A supervised learning approach with application to rehabilitation robotics," *IEEE Trans. Robot.*, vol. 36, no. 3, pp. 789–801, Jun. 2020.
- [20] N. Hogan, "Impedance control: An approach to manipulation," in *Proc. Amer. Control Conf.*, 1984, pp. 304–313.
- [21] S. K. Banala, S. K. Agrawal, S. H. Kim, and J. P. Scholz, "Novel gait adaptation and neuromotor training results using an active leg exoskeleton," *IEEE/ASME Trans. Mechatron.*, vol. 15, no. 2, pp. 216–225, Apr. 2010.
- [22] Y. Mao, X. Jin, G. Gera Dutta, J. P. Scholz, and S. K. Agrawal, "Human movement training with a cable driven arm exoskeleton (CAREX)," *IEEE Trans. Neural Syst. Rehabil. Eng.*, vol. 23, no. 1, pp. 84–92, Jan. 2015.
- [23] A. Duschau-Wicke, J. Von Zitzewitz, A. Caprez, L. Lunenburger, and R. Riener, "Path control: A method for patient-cooperative robot-aided gait rehabilitation," *IEEE Trans. Neural Syst. Rehabil. Eng.*, vol. 18, no. 1, pp. 38–48, Feb. 2010.
- [24] L. L. Cai et al., "Implications of assist-as-needed robotic step training after a complete spinal cord injury on intrinsic strategies of motor learning," *J. Neurosci.*, vol. 26, no. 41, pp. 10564–10568, 2006.
- [25] J. Zhang and C. C. Cheah, "Passivity and stability of human–robot interaction control for upper-limb rehabilitation robots," *IEEE Trans. Robot.*, vol. 31, no. 2, pp. 233–245, Apr. 2015.
- [26] X. Li, Y. Pan, G. Chen, and H. Yu, "Multi-modal control scheme for rehabilitation robotic exoskeletons," *Int. J. Robot. Res.*, vol. 36, nos. 5–7, pp. 759–777, 2017.
- [27] S. Jezernek, G. Colombo, and M. Morari, "Automatic gait-pattern adaptation algorithms for rehabilitation with a 4-Dof robotic orthosis," *IEEE Trans. Robot. Autom.*, vol. 20, no. 3, pp. 574–582, Jun. 2004.
- [28] A. U. Pehlivan, F. Sergi, and M. K. O'Malley, "A subject-adaptive controller for wrist robotic rehabilitation," *IEEE/ASME Trans. Mechatron.*, vol. 20, no. 3, pp. 1338–1350, Jun. 2015.
- [29] E. T. Wolbrecht, V. Chan, D. J. Reinkensmeyer, and J. E. Bobrow, "Optimizing compliant, model-based robotic assistance to promote neurorehabilitation," *IEEE Trans. Neural Syst. Rehabil. Eng.*, vol. 16, no. 3, pp. 286–297, Jun. 2008.
- [30] E. Burdet, R. Osu, D. W. Franklin, T. E. Milner, and M. Kawato, "The central nervous system stabilizes unstable dynamics by learning optimal impedance," *Nature*, vol. 414, no. 6862, pp. 446–449, 2001.
- [31] C. Yang, G. Ganesh, S. Haddadin, S. Parusel, A. Albu-Schaeffer, and E. Burdet, "Human-like adaptation of force and impedance in stable and unstable interactions," *IEEE Trans. Robot.*, vol. 27, no. 5, pp. 918–930, Oct. 2011.
- [32] S.-H. Zhou, J. Fong, V. Crocher, Y. Tan, D. Oetomo, and I. Mareels, "Learning control in robot-assisted rehabilitation of motor skills—A review," *J. Control Decis.*, vol. 3, no. 1, pp. 19–43, 2016.
- [33] M. W. Spong, "Modeling and control of elastic joint robots," *J. Dyn. Sys., Meas., Control*, vol. 109, no. 4, pp. 310–318, 1987.
- [34] H. K. Khalil and J. W. Grizzle, *Nonlinear Systems*, vol. 3. Upper Saddle River, NJ, USA: Prentice-Hall, 2002.
- [35] H. Yu, S. Huang, G. Chen, and N. Thakor, "Control design of a novel compliant actuator for rehabilitation robots," *Mechatronics*, vol. 23, no. 8, pp. 1072–1083, 2013.
- [36] H. Vallery, J. Veneman, E. Van Asseldonk, R. Ekkelenkamp, M. Buss, and H. Van Der Kooij, "Compliant actuation of rehabilitation robots," *IEEE Robot. Autom. Mag.*, vol. 15, no. 3, pp. 60–69, Sep. 2008.
- [37] S. Balasubramanian, R. Colombo, I. Sterpi, V. Sanguineti, and E. Burdet, "Robotic assessment of upper limb motor function after stroke," *Amer. J. Phys. Med. Rehabil.*, vol. 91, no. 11, pp. S255–S269, 2012.
- [38] L. Roveda, N. Iannacci, F. Vicentini, N. Pedrocchi, F. Braghin, and L. M. Tosatti, "Optimal impedance force-tracking control design with impact formulation for interaction tasks," *IEEE Robot. Autom. Lett.*, vol. 1, no. 1, pp. 130–136, Jan. 2016.
- [39] P. Tomei, "A simple PD controller for robots with elastic joints," *IEEE Trans. Autom. Control*, vol. 36, no. 10, pp. 1208–1213, Oct. 1991.
- [40] D. J. Braun et al., "Robots driven by compliant actuators: Optimal control under actuation constraints," *IEEE Trans. Robot.*, vol. 29, no. 5, pp. 1085–1101, Oct. 2013.
- [41] A. Albu-Schäffer and C. O. F. Petit, "Energy shaping control for a class of underactuated Euler-Lagrange systems," *IFAC Proc. Vol.*, vol. 45, no. 22, pp. 567–575, 2012.
- [42] A. T. Massoud and H. A. ElMaraghy, "Model-based motion and force control for flexible-joint robot manipulators," *Int. J. Robot. Res.*, vol. 16, no. 4, pp. 529–544, 1997.
- [43] J. H. Chow, *Time-Scale Modeling of Dynamic Networks With Applications to Power Systems*. New York, NY, USA: Springer, 1982.
- [44] M. W. Spong, "Adaptive control of flexible joint manipulators," *Syst. Control Lett.*, vol. 13, no. 1, pp. 15–21, 1989.
- [45] P. Kokotović, H. K. Khalil, and J. O'reilly, *Singular Perturbation Methods in Control: Analysis and Design*. Philadelphia, PA, USA: SIAM, 1999.
- [46] M. Babaiali, S. H. Mahdioun, P. Jaryani, and M. Yazdani, "A review of technological and clinical aspects of robot-aided rehabilitation of upper-extremity after stroke," *Disabil. Rehabil.: Assistive Technol.*, vol. 11, no. 4, pp. 263–280, 2016.



**Shuaishuai Han** received the Ph.D. degree in control science and engineering from the Nanjing University of Science and Technology, Nanjing, China, in 2021.

He is currently a Postdoctoral Researcher with the National University of Singapore, Singapore. His current research interests include the robot-assistive rehabilitation strategies, control of rehabilitation robotics, and series-elastic-actuator-driven robots.



**Haoping Wang** (Senior Member, IEEE) received the Ph.D. degree in automatic control from the Lille University of Science and Technology (LUST), Lille, France, in 2008.

He is currently Professor with the School of Automation, Nanjing University of Science and Technology, Nanjing, China, a Deputy Director of the Sino-French Engineering School, and a Scientific and Executive Director of the Sino-French International Joint Laboratory of Automatic Control and Signal Processing, Nanjing University of Science and Technology. He was a Research Fellow with MIS Laboratory, Picardie University, Amiens, France, and with the Laboratoire d'Automatique, Génie Informatique et Signal, LUST. His research interests include the theory and applications of hybrid systems, visual servo control, observation design, rehabilitation and power augmentation lower limb exoskeletons robotics, friction modeling and compensation, modeling and control of diesel engines, biotechnological processes, and wind turbine systems.



**Haoyong Yu** (Senior Member, IEEE) received the B.S. and M.S. degrees from Shanghai Jiao Tong University, Shanghai, China, in 1988 and 1991, respectively, and the Ph.D. degree from the Massachusetts Institute of Technology, Cambridge, MA, USA, in 2002, all in mechanical engineering.

He is currently an Associate Professor with the Department of Biomedical Engineering, National University of Singapore, Singapore. His research interests include medical robotics, rehabilitation engineering and assistive technologies, and system dynamics and control.